

Measurements of intensity scintillations and probability density functions of retroreflected broadband 980-nm laser light in atmospheric turbulence

Frederic M. Davidson, MEMBER SPIE
Stéphane Bucaille
 The Johns Hopkins University
 Department of Electrical and Computer
 Engineering
 Baltimore, Maryland 21218

G. Charmaine Gilbreath, MEMBER SPIE
Eun Oh
 U.S. Naval Research Laboratory
 Remote Sensing Division
 Washington, DC 20375

Abstract. Intensity scintillation variances and intensity probability density functions (PDFs) were experimentally measured for broadband (2 nm), 980-nm laser light reflected by two or more corner cube retroreflectors as a function of retroreflector lateral spacing over a short (75 m) atmospheric optical path. The PDFs transitioned from broad double-peaked beta-shaped densities to lognormal as the retroreflector spacing was increased to exceed the optical field's lateral coherence length. Specific spacing for a given average atmospheric structural C_n^2 eliminated interference between the light beams returned by the retroreflectors.
 © 2004 Society of Photo-Optical Instrumentation Engineers. [DOI: 10.1117/1.1795259]

Subject terms: optical communications; coherence; atmospheric optics; turbulence; retromodulators; modulating retroreflectors.

Paper 030556 received Nov. 6, 2003; revised manuscript received Feb. 15, 2004; accepted for publication Apr. 20, 2004.

1 Introduction

High-power, low-coherence-volume lasers are useful in free-space atmospheric optical communication links. For some applications, retromodulators can be useful for optical terminals in asymmetric links.^{1,2} In applications typically requiring transmission over longer ranges, an array of devices is sometimes necessary for a wider field of regard to close a given link. However, in applications where compact arrays are required, partial coherence can cause losses due to interference effects between colocated retroreflectors.

For such a link propagating in the atmosphere, two effects can contribute to channel degradation. The first is scintillation and turbulence, and the second is partial spatial coherence. The latter manifests itself as constructive or destructive interference of the intensity-modulated light reflected from each element in the retroreflector array. In order to mitigate this effect, each retroreflector should be located in a different coherence volume of the transmitted light beam. Otherwise, additional intensity fluctuations due to the coherent interference between the retroreflected light beams will be present in the returned beam. This effect will combine with scintillations induced by atmospheric turbulence and further degrade the channel below the level caused by the turbulence alone. This problem sets the stage for our initial investigation into how to characterize and separate out these effects through such a channel.

The use of high-power, broad-linewidth (≈ 2 nm) 980-nm laser diodes is particularly attractive for this application. The very small coherence volume associated with such lasers makes it possible to space the individual retroreflectors closely while still locating them in separate coherence cells.

This paper reports the results of measurements of intensity fluctuations as a function of retroreflector spacing for ranges up to 100 m using a continuous-wave laser. A 980-nm laser diode that had a 2-nm bandwidth was used as the source. The retroreflectors were spaced in a plane normal to the beam propagation. Intensity probability density functions (PDFs) were measured for the returned light reflected by a single retroreflector, by a pair of retroreflectors equally spaced from the laser beam center, and by up to six retroreflectors symmetrically located about the beam center. The results indicate that for a sufficiently large spacing between two or more retroreflectors, the intensity PDFs were always lognormal. In the case of two closely spaced retroreflectors, the intensity PDFs were U-shaped (or beta-shaped) densities³ that eventually became lognormal as the spacing between the retroreflectors increased to the point where the optical fields reflected from them became statistically independent of each other.

2 Theoretical Considerations

The geometry of the problem is shown in Fig. 1. It is essentially the configuration of a monostatic laser radar, in that the transmitter and receiver are colocated, but there are two or more reflectors, rather than just one. Furthermore, the return light paths from the retroreflectors are not completely overlapping. Consequently, the amplitude and phase fluctuations of the return light from each reflector are influenced by both folded path and reciprocal path contributions.⁴ At the receiver, there will also be amplitude and phase variations due to constructive and destructive interference between the beams returned by the retroreflectors if they are not located in completely independent coherence volumes of the illuminating beam.

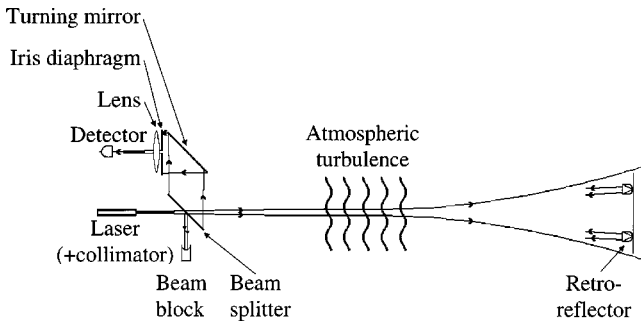


Fig. 1 Block diagram of experimental apparatus.

The expected lateral coherence distance of the illumination beam at the plane $z=L$ of the target retroreflectors is given by⁵

$$\frac{\Gamma_2(d,L)}{\Gamma_2(0,L)} = \exp \left[-\frac{1}{4} \Lambda \left(\frac{kd^2}{L} \right) - \frac{3}{8} a \left(\frac{qkd^2}{L} \right)^{5/6} \right], \quad (1)$$

where d is the transverse distance between the field points and k is the wave vector. The other quantities are $q = 1.22(\sigma_1^2)^{6/5}$, the Rytov variance $\sigma_1^2 = 1.23C_n^2 k^{7/6} L^{11/6}$, $\Lambda = 2L/kW^2(L)$, $a = (1 - \Theta^{8/3})/(1 - \Theta)$, and $\Theta = 1 + L/R(L)$, where the Gaussian beam waist and radius of curvature at distance L are denoted by $W(L)$ and $R(L)$, respectively. The lateral spatial coherence length is obtained by finding the value $d=d_c$ that renders the argument of the exponential in Eq. (3) equal to -1 . For these experiments, this distance is on the order of a few centimeters for the path lengths and C_n^2 values [$\approx (1$ to $5) \times 10^{-14} \text{ m}^{-2/3}$] of our measurements. The receiver beam parameters were $\Lambda=0.0045$ [$W(L)=7.54 \text{ cm}$] and $\Theta=0.005$ [$R(L) \approx L=75 \text{ m}$].

There are two additional phenomena that influence intensity scintillation levels at the receiver. The first is residual turbulence scintillation (RTS),⁶ which arises when the size of the retroreflector (or scattering particle) is small compared to the intensity fluctuation correlation scale, $l_I = \sqrt{\lambda L/2\pi}$, which is about 3.4 mm for these experiments. The diameter of the retroreflectors used was 6 mm, so the reflected light could not be considered as arising from either a point or an extended (diameter $\gg l_I$) source. Consequently, the RTS contribution to the intensity scintillation at the receiver will be somewhat less than values theoretically predicted for a point scatterer. The other effect is enhanced backscatter (EBS), also known as the backscatter amplification effect.⁴ This effect manifests itself as an increase in mean irradiance at the receiver due to correlations between the illuminating and return beams that traverse the same optical path but in opposite directions. For a point reflector illuminated by a spherical wave, the enhancement factor is given by $(0.5C_n^2 k^{7/6} L^{11/6})^{1/2}$, or about 0.07 for these experiments. The short path lengths and weak turbulence conditions render EBS effects negligible for these measurements.

A correct theoretical description of the total field incident on the receiver would involve propagation of the reflected fields from the extended sources (the individual retroreflectors), whose cross-sectional areas were a

considerable fraction of the spatial coherence length of the illuminating optical field, back through the turbulent channel over path lengths that were only partially overlapping. The intensity scintillation at a point in the receiver plane would therefore involve spatial integrals of the fourth-order field correlation function of the atmospherically corrupted illuminating field. The total field at the receiver consists of the sum of only a small number of reflected fields, one from each retroreflector. It is doubtful if central-limit-theorem arguments could be used to model the total return field as a Gaussian stochastic process in order to express fourth-order coherence functions in terms of second-order coherence functions.

Furthermore, the very short temporal coherence time of the laser source limits the interference effects to points in the receiver plane that have optical path lengths to each retroreflector that are the same to within one longitudinal coherence length of the optical source beam. The PDF of the optical intensity at a point in an interference pattern formed between two independent narrow-linewidth optical sources, in the absence of fading, is U-shaped. If the amplitudes of the two sources are also random, the PDF becomes beta-shaped: the sharp edges of the U are broadened. In this experiment, even if we knew the exact form of the PDF for the field amplitude and phase of the retroreflected fields, we could not use convolution to obtain the PDF of the total field intensity at the receiver, because the field components are not statistically independent. However, in the absence of interference effects, the convolution of two lognormal PDFs is approximately a lognormal PDF.⁷

These considerations render a proper theoretical calculation of the expected results well beyond the scope of this paper. The effects of the inner scale of turbulence have not been included.⁸ About all that can be said is that the interference between the two (or more) retroreflected beams will add to the intensity scintillation variance in the receive plane to produce a larger overall intensity variance than would occur if the retroreflected beams were statistically independent. An indirect indication of the lateral coherence distance in the plane of the retroreflectors can be obtained by increasing the distance between them until the normalized intensity variance in the receiver plane has reached its minimum value for fixed receiver aperture size.

The normalized intensity variance in the receiver plane was determined from the statistical properties of the photodetector output photocurrent. The voltage output from the photodetector is related to the photocurrent produced as $v_0(t) = G_V i(t)$, where G_V is the transimpedance gain. The photocurrent is related to the total optical power incident of the photodiode by $i(t) = RI(t) = (e\eta/hf)I(t)$, where R is the photodiode responsivity, e is the charge of one electron, η is the dimensionless quantum efficiency of the photodiode, and hf is the photon energy.

The mean and variance of the output voltage from the photodetector are given by⁹

$$\langle v_0(t) \rangle = G_V R \int \langle I(t') \rangle h(t-t') dt', \quad (2)$$

$$\sigma_v^2 = G_v^2 e R \int \langle I(t') \rangle h^2(t-t') dt' + G_v^2 R^2 \int \int K(r,s) \times h(t-r)h(t-s) dr ds, \quad (3)$$

where all integrals extend from $-\infty$ to ∞ . The impulse response function of the combination of the photodiode and the transimpedance amplifier is $h(t-t')$, and the optical intensity covariance is $K(r,s) = \langle I(r)I(s) \rangle - \langle I(r) \rangle \langle I(s) \rangle$.

In this case, $h(t-t')$ is causal and of sufficiently large bandwidth (50 kHz) that $K(r,s)$ remains constant over the time scale over which $h(t-r)h(t-s) \neq 0$. Under these conditions, the normalized voltage variance becomes

$$\frac{\sigma_v^2}{\langle v \rangle^2} = \frac{2Be}{R\langle I \rangle} + \frac{\sigma_I^2}{\langle I \rangle^2}, \quad (4)$$

where $2B$ represents an effective bandwidth given by $\int h^2(t)dt / (\int h(t)dt)^2$. The first term on the right-hand side of Eq. (4) represents the shot noise associated with the photodetection process, and the second is the normalized variance of the light intensity fluctuations caused by the atmospheric turbulence. In the absence of optical intensity fluctuations, Eq. (4) reduces to just the variance due to shot noise, i.e., the fluctuations in photocurrent due to the Poisson-distributed number of photons in a constant-intensity optical field.

3 Experimental Details

The experimental configuration is shown in Fig. 1. The optical train consisted of the laser transmitter and collimator, the beamsplitter, the turning mirror, the focusing lens and aperture stop, and the combined photodiode and transimpedance current amplifier. Light from the 980-nm laser diode source was coupled to the collimator lens with a single-mode fiber and directed to the target array of retroreflectors by passing through a 50:50 beamsplitter. The beamsplitter redirected light reflected by the retroreflectors to a 5-cm-diameter, 10-cm-focal-length lens via the turning mirror. The effective aperture of the focusing lens was controlled with an iris diaphragm, which could be adjusted from 2.5 to 45 mm. A photograph of the transmitter/receiver board is shown in Fig. 2.

The detector unit was a PDA 400 and was operated at its maximum gain setting of 750 kV/A. Background light was eliminated with the use of a 10-nm bandpass interference filter. The electrical bandwidth was 50 kHz, and the responsivity R of the photodiode was 0.65 A/W at 980 nm. The output voltage was sampled by a National Instruments data acquisition board at the rate of 10^4 10-bit samples per second for up to 10 s, and the digitized values stored in data files on a portable computer.

Measurements in these experiments were made only under conditions such that the average output voltage levels exceeded 0.1 V, which corresponds to a value of $R\langle I \rangle = 0.13 \mu\text{A}$. The effective bandwidth of $2B = 50 \text{ kHz}$ gives a value of 6×10^{-8} for the shot noise contribution, which is 4 or more orders of magnitude smaller than the turbulence-induced expected values of the normalized optical intensity

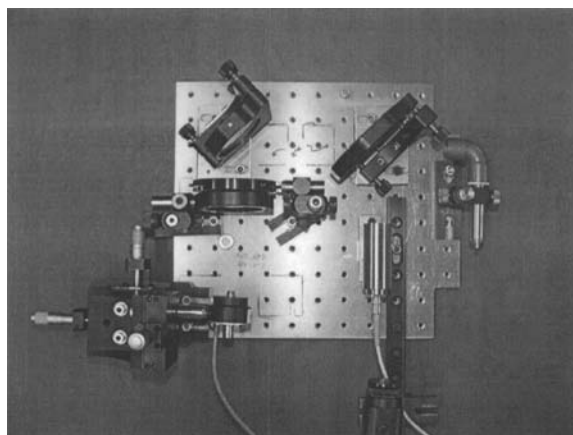


Fig. 2 Photograph of laser transmitter-receiver board.

variance. Therefore Eq. (4) reduces to just the variance from just the turbulence-induced intensity fluctuation.

The Gaussian laser beam was centered on the target board. The 2-nm bandwidth of the 980-nm laser gives a laser temporal coherence time of $\tau = \lambda^2 / (c \Delta\lambda) = 1.6 \times 10^{-12} \text{ s}$, for a longitudinal coherence length of $c\tau = 0.5 \text{ mm}$. Measurements of the angular divergence of the collimated laser beam yielded a value of about 1 mrad. The diameter of the individual retroreflectors was 6 mm. At one-way path lengths of 50 to 100 m, the beam diameter at the plane of the retroreflectors was on the order of 10 cm.

In order to obtain interference between the light reflected from two retroreflectors, the optical path length difference must be kept less than 0.5 mm, the longitudinal coherence length of the laser. This required mounting the retroreflectors on a flat target board and aligning the plane of the target board to within 1 deg of the normal to the propagation direction of the incident beam. A large mirror was mounted flat on the target board immediately adjacent to the center retroreflector. The board itself could be rotated about two axes normal to the direction of beam propagation. A CCD camera mounted on the transmitter board was used to detect the reflections from both the corner cube retroreflectors and the flat mirror. The target board was aligned so that the flat mirror reflected the incident laser beam back onto the beamsplitter on the transmitter board, thereby assuring that the plane of the target board was normal to the beam propagation direction to within 1 deg. Once the target board was aligned, the flat mirror was covered so that only the retroreflectors were illuminated.

The atmospheric path lengths used had to be kept short because of the limited output power output from the laser used (100 to 300 mW), the small areas of the retroreflectors, and the 6-dB power loss due to the beamsplitter. The last-mentioned could, in principle, be eliminated through the use of a polarization-state-sensitive beamsplitter and quarter-wave plate. The corner cube retroreflectors, however, alter the polarization state of the reflected beam. Another alternative is to replace the beamsplitter with an annular mirror that would transmit all of the laser light but would not reflect the exact center of the return beam. In order to keep the interpretation of the results of the measurements as unambiguous as possible, neither of these alternatives was used.

A scintillometer was used to measure values of the refractive index constant C_n^2 . The atmospheric path traversed a grassy area in full sunlight. These conditions typically gave measured values of C_n^2 in the range 10^{-13} to $10^{-14} \text{ m}^{-2/3}$. At a wavelength of 980 nm, path lengths between 50 and 100 m resulted in easily measured values of the normalized intensity scintillation and spatial coherence length.

The atmospheric-turbulence-induced intensity scintillation levels, which increase as $C_n^2 k^{7/6} L^{11/6}$,⁴ were quite small for the measured values of C_n^2 , and values of $\sigma_I^2 / \langle I \rangle^2$ were typically on the order of 10^{-3} . The 10-bit quantization of the photodetector output signals had digital quantization-noise variance on the order of 10^{-5} . The spatial coherence length, on the other hand, decreases with increasing path length as $(C_n^2 k^2 L)^{-3/5}$ and was typically a few centimeters.

For a fixed lens aperture size, data were recorded from different retroreflector distributions. A reference was taken with a single retroreflector located at the center of the beam. Data were then taken from two retroreflectors symmetrically displaced from the beam centerline by a distance d . The center-to-center distance between retroreflectors was $2d$. Data were also recorded from three or more retroreflectors all equally displaced from the beam center but not from each other. This procedure was repeated for aperture diameters of 3 to 30 mm.

The normalized intensity variance and PDF for normalized intensity values were computed for each data file from records of length 100,000 (10-s samples). Spatial coherence lengths of the optical field at the target board could be found by observing the decrease in the normalized variance of the light returned by two retroreflectors as the separation between them increased.

It was, of course, not possible to control values of C_n^2 for these measurements. Many data files were taken, and those for which it was apparent that this parameter had changed substantially over the course of the 10 s of data acquisition were discarded. It was often the case that C_n^2 varied by less than a factor of 2 over tens of minutes.

In order to determine the PDF of the return light intensity, each recorded data file was processed by computing the mean value of the 10-bit digitized samples of the PDA-400 output voltage v . Each data point was then normalized by the mean; the result is hereafter denoted as z_i . A histogram of the normalized data was computed with bin size $\Delta z = (5V/1024) / \langle v \rangle$. The experimentally measured PDF for z was found by dividing the total number of occurrences of values of z_i in the range $(z_i, z_i + \Delta z)$ by the total number of data points in the file. The experimentally measured PDF was then plotted as a function of z with each data point located at $z_i + (\Delta z/2)$.

In order to compare the experimentally measured PDF with a lognormal PDF, a third data file consisting of the values $\ln z_i$ was created. The mean and variance of these data points were computed and then used in the theoretical expression for the lognormal PDF:

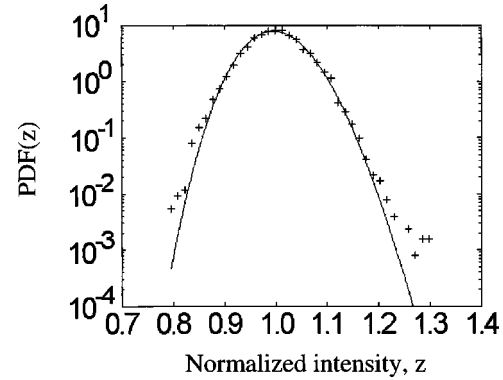


Fig. 3 Measured PDF for normalized intensity of light reflected by a single retroreflector located at the beam center over a 75-m atmospheric path. Solid curve represents lognormal PDF with $\sigma_{\ln z}^2 = 2.58 \times 10^{-3}$ and step size $\Delta z = 1.3 \times 10^{-2}$.

$$p(z_i) = \frac{1}{(2\pi\sigma_{\ln z}^2)^{1/2}} \frac{1}{z_i} \exp\left[-\frac{(\ln z_i - \langle \ln z \rangle)^2}{2\sigma_{\ln z}^2}\right]. \quad (5)$$

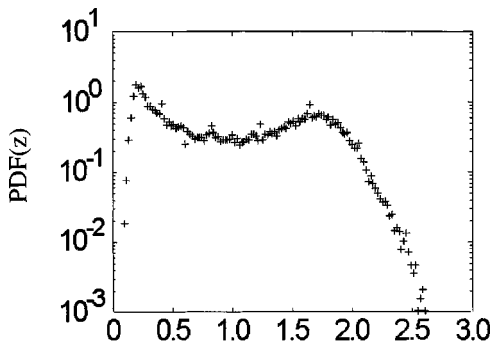
4 Results

A typical result for light reflected by a single retroreflector located at the center of the beam is shown in Fig. 3, where the experimentally determined points of the PDF lie very close to the curve predicted by Eq. (5). Points in the wings of the PDF that lie off the curve represent very few occurrences of those particular values of z_i . The actual number of events can be computed by multiplying the ordinate value by $(\Delta z)N$, where N is the total number of data points in the file, typically 10^5 . For this figure, these points represent one event at a PDF value of 10^{-3} . The measured variance $\sigma_{\ln z}^2 = 2.58 \times 10^{-3}$ for this beam divergence, beam waist, and distance gives an inferred value of $C_n^2 = 2 \times 10^{-14} \text{ m}^{-2/3}$, found by using the formulas in Table 2 of Ref. 10. This value is well within the range of those registered by the scintillometer.

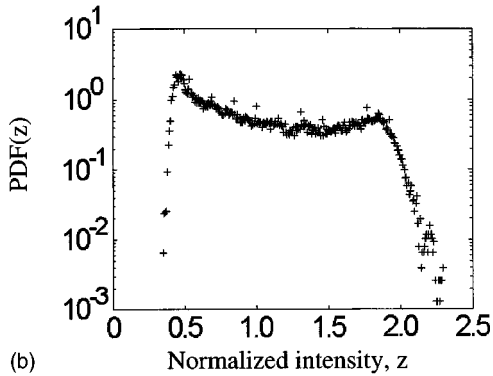
The PDF for light reflected by two closely spaced retroreflectors is clearly not lognormal, as shown by the data of Figs. 4(a) to 4(d). These graphs are plots of experimentally determined PDFs with the receiver aperture diameter D_R as a parameter for a fixed retroreflector spacing of 10 mm.

Figures 4(a) to 4(d) show the experimentally obtained PDFs for a retroreflector spacing of 10 mm and a range of receiver aperture diameters from 3 to 30 mm. The PDFs are always double-peaked functions with the height and symmetry of the peaks dependent on the exact turbulence conditions. The data indicate the presence of interference between the retroreflected beams, which makes the PDF of the intensity in the receiver plane decidedly not lognormal in shape. Figures 5 and 6 show transition to lognormal behavior as the retroreflector spacing is increased with the lens aperture diameter as a parameter.

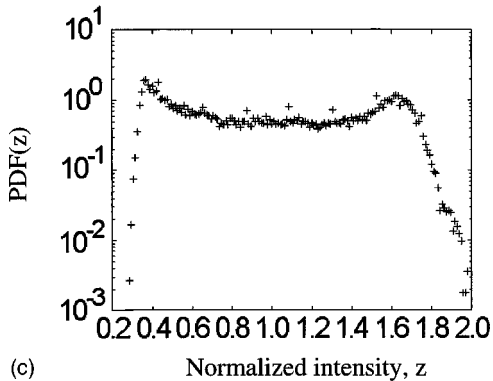
Figures 4 through 6 show the passage from double-peaked to lognormal as the retroreflector spacing is increased, and/or as the aperture diameter of the receiver focusing lens is increased. The solid lines in these figures represent a lognormal PDF as computed from Eq. (5) using



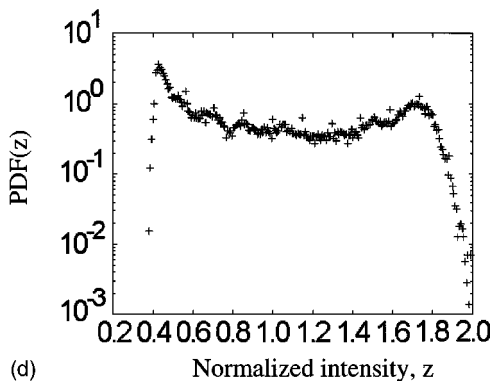
(a)



(b)

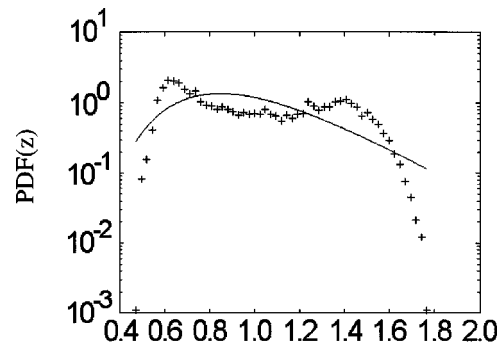


(c)

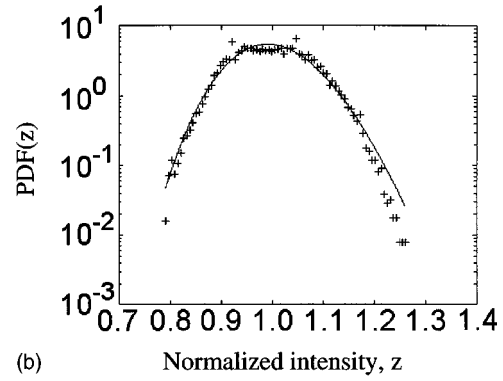


(d)

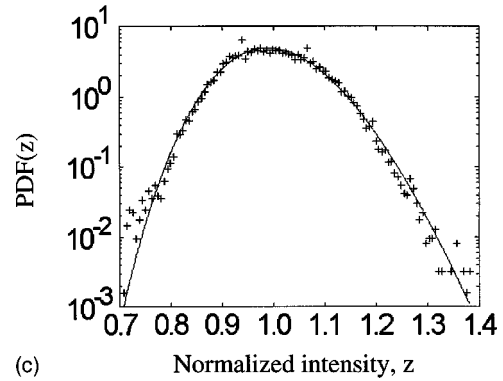
Fig. 4 Experimentally determined PDF(z) versus z for retroreflector spacing of 10 mm and lens aperture diameters of (a) 3 mm, (b) 10 mm, (c) 20 mm, and (d) 30 mm.



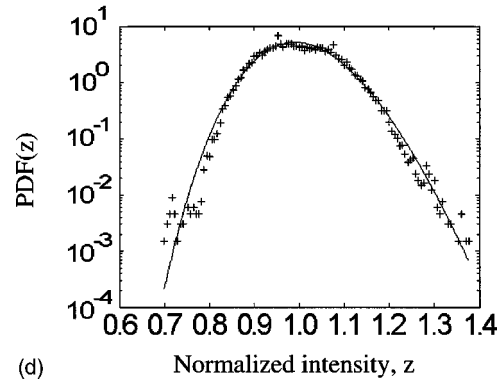
(a)



(b)



(c)



(d)

Fig. 5 Experimentally determined PDF(z) versus z for a retroreflector spacing of 20 mm with lens aperture diameter as a parameter. Solid curves represent lognormal PDF. Parameter values are (a) $D_R=3$ mm, $\sigma_{\ln z}^2=1.09 \times 10^{-1}$, $\Delta z=2.39 \times 10^{-2}$; (b) $D_R=10$ mm, $\sigma_{\ln z}^2=5.38 \times 10^{-3}$, $\Delta z=5.96 \times 10^{-3}$; (c) $D_R=20$ mm, $\sigma_{\ln z}^2=6.61 \times 10^{-3}$, $\Delta z=6.06 \times 10^{-3}$; (d) $D_R=30$ mm, $\sigma_{\ln z}^2=6.02 \times 10^{-3}$, $\Delta z=5.89 \times 10^{-3}$.

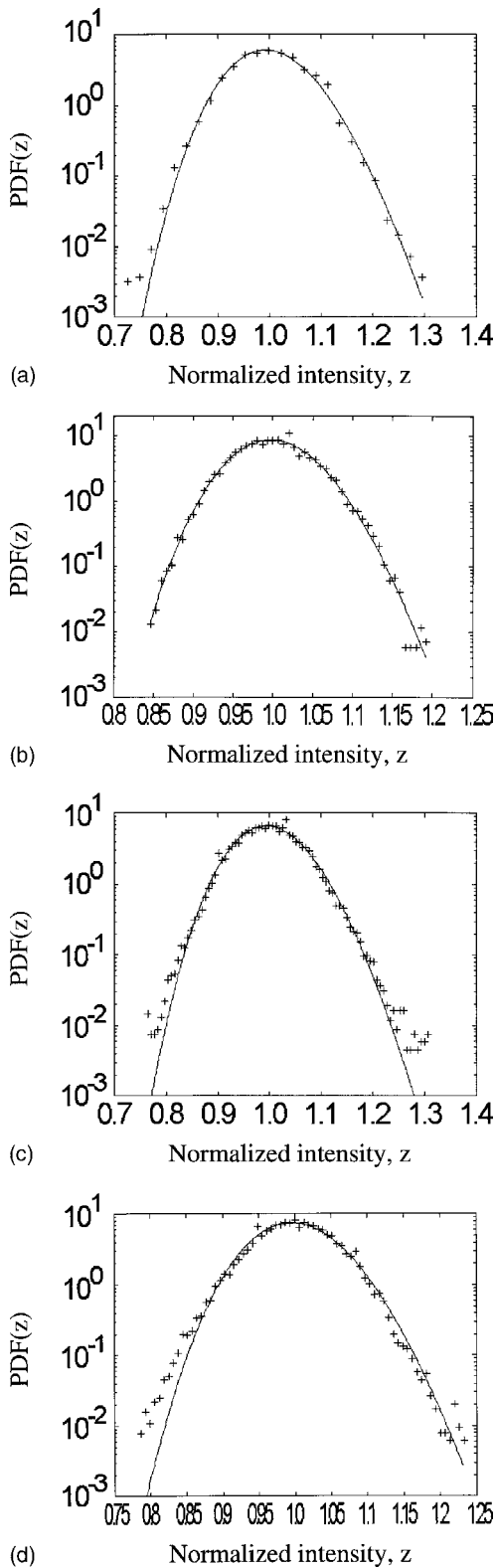


Fig. 6 Experimentally determined PDF(z) versus z for a retroreflector spacing of 60 mm with lens aperture diameter as a parameter. Solid curves represent lognormal PDF. Parameter values are (a) $D_R=3$ mm, $\sigma_{\ln z}^2=4.36 \times 10^{-3}$, $\Delta z=2.28 \times 10^{-2}$; (b) $D_R=10$ mm, $\sigma_{\ln z}^2=2.07 \times 10^{-3}$, $\Delta z=6.65 \times 10^{-3}$; (c) $D_R=20$ mm, $\sigma_{\ln z}^2=3.63 \times 10^{-3}$, $\Delta z=6.52 \times 10^{-3}$; (d) $D_R=30$ mm, $\sigma_{\ln z}^2=2.84 \times 10^{-3}$, $\Delta z=6.47 \times 10^{-3}$.

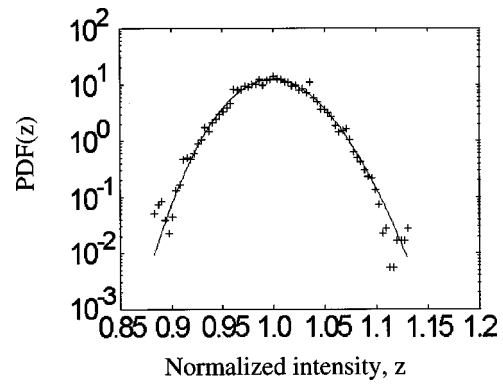


Fig. 7 Experimentally determined PDF(z) versus z for light reflected by two retroreflectors spaced 10 mm apart in the transverse direction and 3 cm apart in the beam propagation (longitudinal) direction.

values of $\langle \ln z \rangle$ and $\sigma_{\ln z}^2$ determined directly from the data file. The values of $\sigma_{\ln z}^2$ represent the variation in values of C_n^2 from data file to data file. These ranged in value from about 1×10^{-14} to about $5 \times 10^{-14} \text{ m}^{-2/3}$ for the data files that fit a lognormal PDF model.

Figure 7 shows an experimentally measured PDF for the case of two retroreflectors spaced 10 mm apart but separated by several centimeters in the beam propagation direction so that the retroreflectors were in different longitudinal coherence volumes. These PDFs were always lognormal, regardless of the lens aperture diameter.

Through Eq. (1), the measurements described give an indirect indication of the lateral spatial coherence length of the beam at the retroreflectors, through the dependence on retroreflector spacing, and at the receiver, through the behavior of the PDFs as a function of aperture size. The Gaussian beam used in these experiments had the values $\Theta=0.005$ and $\Lambda=4 \times 10^{-3}$ at $L=75$ m. Figure 8 shows the behavior of d_c as found from Eq. (1) over the range $10^{-15} \leq C_n^2 \leq 10^{-13}$. This figure indicates that the lateral coherence distance should be on the order of 15 to 55 mm and is very consistent with the behavior of the experimentally determined PDFs.

Finally, the behavior of the variance of the intensity fluctuations of the retroreflected light is shown in Fig. 9.

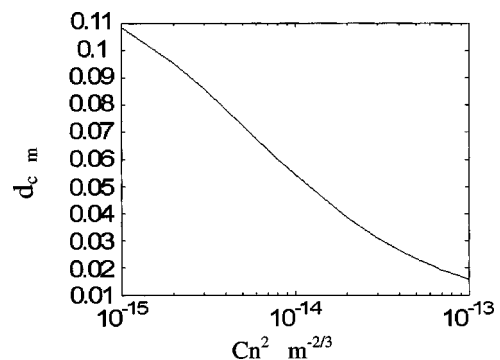


Fig. 8 Computed values of optical field lateral coherence length ρ_c as determined from Eq. (1), as a function of the turbulence parameter C_n^2 .

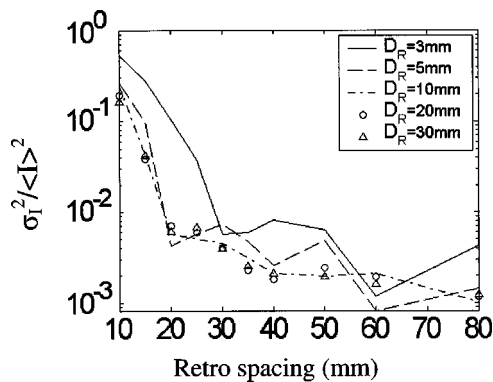


Fig. 9 Experimentally measured values of normalized intensity variance $\sigma_I^2/\langle I \rangle^2$ as a function of retroreflector spacing with lens aperture diameter as a parameter. For the lognormal PDFs, $\sigma_I^2/\langle I \rangle^2 = \exp(4\sigma_\chi^2) - 1$.

The behavior is independent of the form of the PDF and is shown as a function of retroreflector spacing. The plots show the normalized intensity variance $\sigma_I^2/\langle I \rangle^2$, as determined directly from the data files, versus retroreflector spacing for lens aperture diameters of 3, 5, 10, and 30 mm. If the PDF for the returned light intensity is lognormal, then $\sigma_I^2/\langle I \rangle^2 = \exp(4\sigma_\chi^2) - 1$, where $4\sigma_\chi^2 = \sigma_{\ln z}^2$. Figure 9 shows that in order to operate this system with minimal bit error rate, the retroreflector spacing should be about 60 mm in order for $\sigma_I^2/\langle I \rangle^2$ to reach its minimal value on the order of 10^{-3} , which will also result in a single-peaked lognormal PDF for the normalized optical field intensity.

If more than two retroreflectors are used, the PDF for the photocurrent has no definite form; it is broad, may have multiple peaks, and is not lognormal. Once the spacing between every pair of retroreflectors exceeds the lateral spatial coherence distance, or all individual retroreflectors are located in independent coherence volumes, the PDF for the photocurrent is again lognormal, and a minimal bit error rate should result.

5 Conclusions

The performance of an optical link that uses an array of retroreflectors depends strongly on the placement of the individual retroreflectors in the target plane. Intensity fluctuations arise from coherent interference at the receiver between light beams reflected by the individual retroreflectors and can be mitigated through cognizance of this effect. One solution is to use a laser beam that has a low coherence volume transmitted with minimal divergence angle so that the retroreflectors can be closely spaced, yet located in independent coherence volumes. Broad-linewidth, 980-nm high-power diode lasers appear to be a good candidate for use in these types of systems.

The results of the experimental measurements to indirectly determine lateral coherence distances, reported here, clearly show the evolution of the PDF of light intensity from broad, multiple-peaked densities to single-peaked lognormal densities. The normalized intensity variance in the receiver plane is shown to be determined by both the transmitter Gaussian beam parameter and the atmospheric turbulence levels (which determine d_C), as well as by the spacing between the retroreflectors. The particular laser used here had a coherence volume of approximately $6 \text{ cm}^2 \times 0.5 \text{ mm} = 0.3 \text{ cm}^3$ after propagating 75 m through atmospheric turbulence characterized by values of C_n^2 in the range of 10^{-14} to $10^{-13} \text{ m}^{-2/3}$.

Measurements of the normalized intensity variance for light reflected by two or more retroreflectors can be used to infer the bit error rate performance of an actual communication system using retromodulators. Future work will explore how an array of multiple quantum well (MQW) modulating retroreflectors can be configured to mitigate coherence effects.

Acknowledgments

We would like to thank William S. Rabinovich, David Mozurkewich, Rita Mahon, and Ray Burris for their insights. We would also like to thank the reviewers for their useful comments on the manuscript.

References

1. G. C. Gilbreath, W. S. Rabinovich, T. J. Meehan, M. J. Vilcheck, M. F. Stell, R. Mahon, P. G. Goetz, E. Oh, J. A. Vasquez, K. Cochrell, R. Lucke, and S. Mozersky, "Progress in development of multiple quantum well retromodulators for free-space data links," *Opt. Eng.* **42**(6), 1611–1617 (2003).
2. W. S. Rabinovich, G. C. Gilbreath, R. Mahon, R. Burris, P. Goetz, C. I. Moore, M. Ferraro, J. L. Witdowsky, L. Swingen, E. Oh, and J. Koplow, "Free-space optical communications link at 1550 nm using multiple quantum well modulating retroreflectors over a 1-kilometer range," presented at Ann. Mtg., May 2003, 230.5590, Optical Society of America.
3. A. Papoulis and S. Pillai, *Probability, Random Variables, and Stochastic Processes*, 4th ed., pp. 91–92, McGraw-Hill, New York (2002).
4. L. Andrews, R. Phillips, and C. Hopon, *Laser Beam Scintillations with Applications*, Chap. 9, SPIE Optical Engineering Press, Bellingham, WA (2001).
5. L. Andrews and R. Phillips, *Laser Beam Propagation through Random Media*, Chap. 6, SPIE Optical Engineering Press, Bellingham, WA (1998).
6. M. Belen'kii, "Effect of residual turbulent scintillation and a remote-sensing technique for simultaneous determination of turbulence and scattering parameters of the atmosphere," *J. Opt. Soc. Am. A* **11**, 1150–1158 (1994).
7. R. Barakat, "Sums of independent lognormally distributed random variables," *J. Opt. Soc. Am.* **66**(3), 211–216 (1976).
8. A. Consortini, F. Cochetti, J. H. Churnside, and R. J. Hill, "Inner-scale effect on irradiance variance measured for weak-to-strong atmospheric scintillation," *J. Opt. Soc. Am. A* **10**(10), 2354–2362 (1993).
9. L. Mandel and E. Wolf, *Optical Coherence and Quantum Optics*, pp. 452–457, Cambridge University Press (1995).
10. W. Miller, J. Ricklin, and L. Andrews, "Log-amplitude variance and wave structure function: a new perspective for Gaussian beams," *J. Opt. Soc. Am.* **10**(4), 661–672 (1993).